A global map of uncertainties in satellite-based precipitation measurements

Yudong Tian[1,3] and Christa D. Peters-Lidard[2]

Received 28 October 2010; revised 18 November 2010; accepted 29 November 2010; published 31 December 2010.

[1] A global map of measurement uncertainties in satellite-based precipitation estimates has been produced by computing the variance from an ensemble of six different TRMM-era data sets at daily, 0.25° resolution. This analysis yields a lower-bound estimate of the uncertainties, and a consistent global view of the error characteristics and their regional and seasonal variations, and reveals many undocumented error features over areas with no validation data available. The uncertainties are relatively small (40–60%) over the oceans, especially in the tropics, and over southern South America. There are large uncertainties (100–140%) over high latitudes (poleward of 40° latitude), especially during the cold season. High relative uncertainties are also evident through the seasons over complex terrain areas, including the Tibetan Plateau, the Rockies and the Andes. Coastlines and water bodies also indicate high measurement uncertainty. The estimated global uncertainties also exhibit systematic seasonal, regional as well as rain-rate dependencies, with lowest uncertainties over tropical oceanic regions with strong, convective precipitation, and highest ones over wintery, complex land surfaces with light precipitation. **Citation:** Tian, Y., and C. D. Peters-Lidard (2010), A global map of uncertainties in satellite-based precipitation measurements, *Geophys. Res. Lett.*, *37*, L24407, doi:10.1029/2010GL046008.

1. Introduction

[2] Currently, satellite-based remote sensing is the only practical way to measure precipitation on the global scale. Satellite sensors can cover vast, diverse areas of the Earth's surface such as oceans, deserts and high mountains, which are infeasible to monitor with conventional rain gauges or meteorological radars. Especially since the launch of the Tropical Rainfall Measurement Mission (TRMM) satellite in 1997, we have entered an era to observe global precipitation with an array of sensors aboard multiple satellite platforms, and to produce globally consistent, high-resolution precipitation measurements from the synthesis of these sensors.

[3] Although many satellite-based global precipitation data sets are routinely produced, a quantitative, global picture of their error characteristics is lacking. For example, it is commonly believed that passive microwave (PMW) retrievals of precipitation are more accurate over the ocean than over the land, but global quantification of this hypothesis remains a challenge. In addition, the heterogeneity of the land surface itself also makes the performance of such retrievals vary greatly from region to region, and such variation needs to be determined as well.

[4] The difficulty in assembling a globally consistent error map lies in the lack of gauge or radar coverage over most areas of the Earth's surface. Therefore existing studies have focused on areas where reliable ground-based measurements are available [e.g., *Gottschalck et al.*, 2005; *Ebert et al.*, 2007; *Tian et al.*, 2009; *Sapiano and Arkin*, 2009; *Vila et al.*, 2009]. It is also possible to use the precipitation radar (PR) aboard TRMM to validate other sensors [e.g., *Lin and Hou*, 2008], but PR's coverage is still limited to the tropics and to its narrow swaths.

[5] In this study, a global map of the error uncertainties in satellite-based measurements has been produced. The uncertainties have been estimated as the measurement spread of coincidental and collocated estimates from an ensemble of six different satellite-based data sets, thus providing a globally consistent estimate methodology that does not require surface-based validation data. This approach was proposed by *Adler et al.* [2001] and has recently been used by *Adler et al.* [2009] to produce a tropical rainfall climatology from a three-member ensemble. Many of the global error features we produced are consistent with existing studies over areas with validation data available, while many other features have not been documented before. In addition, the regional, seasonal and rain-rate dependencies of the uncertainties are analyzed. These results can serve not only as estimates of the random errors in these data sets, but also as a measure of the "difficulty" in measuring precipitation by space-borne sensors over various areas of the Earth's surface.

2. Data and Methods

[6] Six high-resolution precipitation data sets were used in this study. They are commonly referred to as 3B42, 3B42RT [*Huffman et al.*, 2007], CMORPH [*Joyce et al.*, 2004; *Janowiak et al.*, 2005], GSMaP [*Okamoto et al.*, 2005; *Kubota et al.*, 2007], PERSIANN [*Hsu et al.*, 1997] and NRL-blended, or NRL for short [*Turk and Miller*, 2005]. Table 1 provides a concise summary of these data sets, including their full names, native spatial and temporal resolutions for the versions used, and the major sensor types that comprise each product.

[7] We selected these data sets because they are all produced from the merging of multiple PMW and infrared (IR) sensors. Such merged products maximize spatial and temporal sampling over the globe, and exhibit higher accuracy

[1]Earth System Science Interdisciplinary Center, University of Maryland, College Park, Maryland, USA.
[2]Hydrological Sciences Branch, NASA Goddard Space Flight Center, Greenbelt, Maryland, USA.
[3]Also at Hydrological Sciences Branch, NASA Goddard Space Flight Center, Greenbelt, Maryland, USA.

0094-8276/10/2010GL046008

Table 1. Summary of Data Sets Used

Data Set	Full Name	Spatial Resolution	Temporal Resolution	Sensor Platforms	References
3B42	TRMM Multi-satellite Precipitation Analysis research product 3B42 Version 6	0.25°	3 h	IR, SSM/I, TRMM, AMSU-B, AMSR-E, gauges	*Huffman et al.* [2007]
3B42RT	TRMM Multi-satellite Precipitation Analysis Real-time experimental product 3B42RT	0.25°	3 h	IR, SSM/I, TRMM, AMSU-B, AMSR-E	*Huffman et al.* [2007]
CMORPH	NOAA Climate Prediction Center (CPC) MORPHing technique	0.25°	3 h	IR, SSM/I, TRMM, AMSU-B, AMSR-E	*Joyce et al.* [2004] and *Janowiak et al.* [2005]
GSMaP	Global Satellite Mapping of Precipitation (GSMaP MVK+ Version 4.8.4)	0.1°	1h	IR, SSM/I, TRMM, AMSU-B, AMSR-E	*Okamoto et al.* [2005] and *Kubota et al.* [2007]
PERSIANN	Precipitation Estimation from Remotely Sensed Information using Artificial Neural Networks	0.25°	3 h	IR, TRMM	*Hsu et al.* [1997]
NRL	Naval Research Laboratory's blended technique	0.25°	3 h	IR, VIS, SSM/I, TRMM, AMSU-B, AMSR-E	*Turk and Miller* [2005]

due to the inter-calibration among the diverse sensors [e.g., *Adler et al.*, 1993]. Though they share many of the input streams from the same sensors (e.g., TRMM), the methods these products use to inter-calibrate, interpolate and combine these input streams vary greatly from product to product.

[8] A period of two years—from 2005 through 2006—was used for this study, during which all the six data sets in our archive overlapped. All the data sets were re-projected to the same 0.25° spatial resolution if needed and aggregated to daily accumulation.

[9] Here uncertainties are defined as the standard deviation among independent measurements of the same physical quantity. The uncertainties in the precipitation measurements were estimated by the following steps. First, we used the six data sets to form an ensemble, and at each grid box and time step we computed the six-member ensemble mean. Then we identified one outlier from the ensemble which deviated most from the ensemble mean, and removed the outlier from the ensemble. Subsequently the ensemble mean was re-computed with the five remaining members. The outlier-removal procedure is to prevent an anomalous member from corrupting the ensemble, and it was performed at each grid box and time step, therefore the outlier is not necessarily always the same member. In practice, our test showed the results thus obtained are not qualitatively different from those without the outlier-removal step. Finally, the standard deviation of the members from the ensemble mean was calculated as an estimate of the measurement uncertainties.

[10] We want to note that the ensemble spread thus determined reflects both systematic errors and random errors. Also due to the small ensemble size and to the fact that the ensemble members are not totally independent, such an approach will underestimate the random errors. With this in

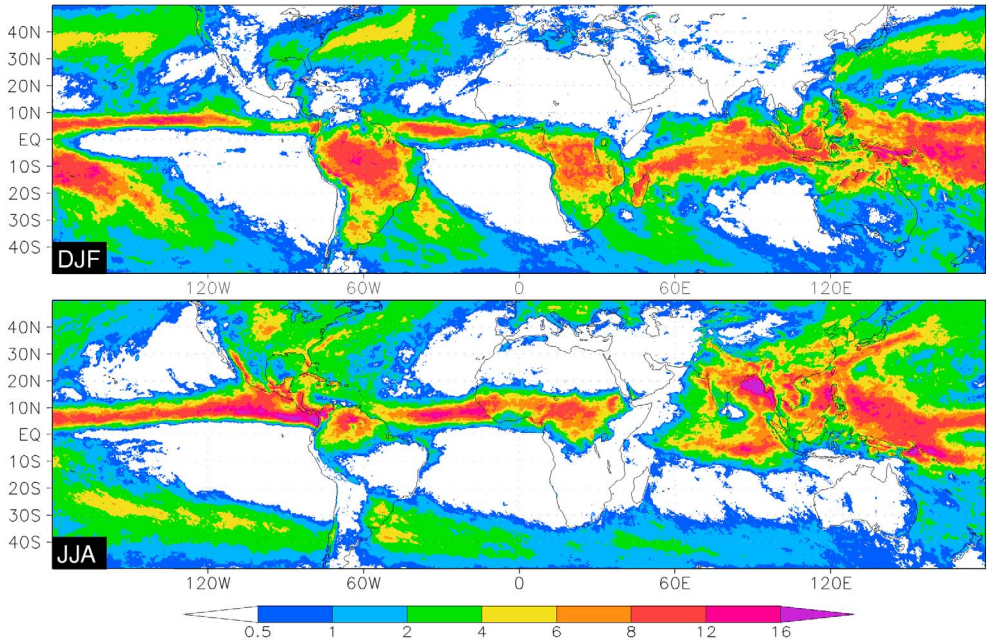

Figure 1. Mean daily precipitation (mm) of the six-member ensemble for boreal (top) winter (DJF) and (bottom) summer (JJA).

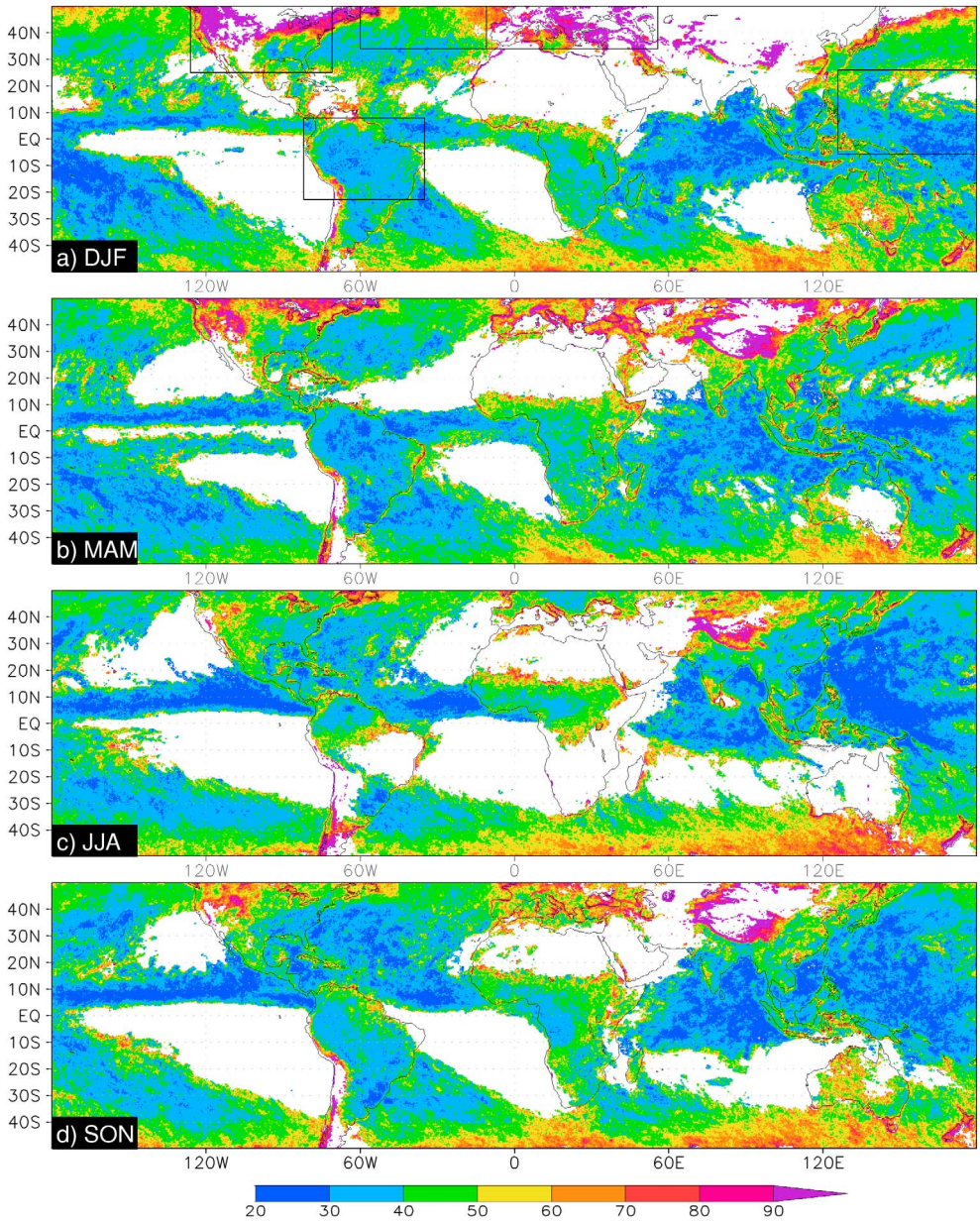

Figure 2. (a–d) Standard deviation from the ensemble mean, as percentage of the mean daily precipitation, averaged for the four seasons, respectively. Areas with mean daily precipitation less than 0.5 mm are shown as blank as they are deemed unreliable. The boxes in Figure 2a delineate the five regions in subsequent studies.

mind, the results nevertheless provide meaningful insight, particularly when we focus on the relative magnitude of the uncertainties across the globe.

3. Results

[11] The mean state of the ensemble was produced and examined first. Figure 1 shows the ensemble-mean daily precipitation, for both the boreal winter (December, January, and February - DJF) and summer (June, July, and August – JJA). Prominent features, such as the precipitation areas associated with the migration of the Inter-tropical Convergence Zone (ITCZ) over Africa, and the Asian Summer Monsoon, are present as expected. The seasonal variation of precipitation over the continental United States (CONUS) is also consistent with surface observations, as shown in previous work cited above.

[12] Although we may place more confidence in the ensemble mean of the global precipitation than in an individual member, the current study does not quantify any systematic errors in the ensemble mean, because no validation data were used. In fact, the systematic errors in the ensemble mean, as well as in each individual member, could be rather large, as seen from existing studies over areas with surface validation data [e.g., *Ebert et al.*, 2007]. Moreover, the systematic errors in each of these satellite-based data sets tend to be similar for summer but differ considerably for

winter over U.S., for example [*Tian et al.*, 2009], thus the systematic errors in the ensemble mean for summer in such cases are not necessarily much smaller from the averaging.

[13] The global uncertainty map for each of the four seasons is shown in Figure 2. Instead of showing the absolute values of the standard deviation from the ensemble mean, we show the relative uncertainties as the ratios between the standard deviation and the ensemble mean precipitation over each grid box. An illustrative picture emerges, giving a clear indication of where these satellite-based products are performing better or worse.

[14] Generally, one sees relatively lower uncertainties over areas with stronger precipitation shown in Figure 1, especially over the tropics. This indicates that the satellite-based retrievals tend to detect and measure strong events better, partially due to the higher signal to noise ratio, and partially due to the favorable convective precipitation regimes for PMW-based measurements. The performance at higher latitudes degrades considerably, especially poleward of 40° latitude. This can be attributed to coverage by fewer sensors (e.g., lack of TRMM coverage), light precipitation events, snowfall, and in the case of land surfaces, snow and ice on the ground which produce a signal similar to precipitation (e.g., Figure 2a). It is also possible that at higher latitudes the larger standard deviations reflect precipitation algorithm differences, as discussed by *Adler et al.* [2001].

[15] In addition, one tends to see lower uncertainties over the ocean than over the land, especially during the local spring season (e.g., Figure 2b for CONUS and Eurasia and Figure 2d for Australia). This is consistent with expectations. However, South America is an exception, especially in its warm season when the uncertainties are comparable with those over ocean surfaces, even at fairly high latitudes.

[16] This global uncertainty map also reveals many fine-scale error features. The Tibetan Plateau, the Rockies and the Andes pose a constant challenge across all seasons, likely due to the orographic precipitation associated with the complex terrain and snow and ice covers on the ground during cold seasons at higher elevations. There are also consistently higher uncertainties along coastlines (e.g., Figure 2b) and over water bodies (e.g., the Great Lakes in Figure 2c), which have been documented in previous studies [e.g., *McCollum and Ferraro*, 2005]. Over Africa there are also uncertainties associated with the ITCZ rainband, especially along its flanks, with amplitudes much higher than its oceanic counterpart over the central Atlantic (Figure 2c).

[17] Uncertainties in the precipitation measurements exhibit strong regional, seasonal, and rate-rate dependencies. To investigate these dependencies, we selected five regions (CONUS, Europe, South America, Northern Atlantic and Western Pacific) delineated in Figure 2a, and compared their uncertainties across different rain rates and over the four seasons (Figure 3). In each region the daily standard deviation values were binned to their ensemble mean rain rates, and the median of the standard deviation values for each bin is plotted.

[18] First, with the land and ocean surfaces over the Northern Hemisphere as two separate regions, Figures 3a and 3b show that the land surfaces exhibit systematically higher uncertainties than the ocean in winter (DJF), especially for light precipitation (<8 mm/d, Figure 3a). The gap between the two surface types narrows down remarkably in summer (JJA), though, except for heavier precipitation (>8 mm/d). The uncertainties for heavier precipitation (>8 mm/d) seem less affected by the season (Figures 3a and 3b).

[19] Among the five regions, CONUS and Europe show much higher uncertainties during winter (Figure 3c), while the other three regions have similar uncertainty amplitudes. However, during summer, the spread over CONUS and Europe is comparable to that of the other three regions (Figure 3d). The latter show very slight seasonal differences, and South America exhibits surprisingly similar uncertainty amplitudes to those of the two oceanic regions (Northern Atlantic and Western Pacific).

[20] For all the regions shown in Figure 3, the relative uncertainties decrease rapidly with the mean precipitation rate, from over 100% at 1 mm/d to less than 30% at 32 mm/d and higher. This is consistent with our observations and explanations in Figures 1 and 2.

[21] Finally, Figures 3e and 3f illustrate the seasonal variations in the uncertainties for two of the five regions. CONUS and Europe show strong seasonal dependencies, with the winter season producing the highest amplitudes and summer the lowest, especially at lower rain rates (<8 mm/d). However, there are significant differences between the two regions: over CONUS the seasonal differences in uncertainties largely disappear at higher rain rates (>8 mm/d, Figure 3e), while over Europe they persist, and the uncertainties in winter are much worse than the other three seasons (Figure 3f). We also examined two other regions, Northern Atlantic and South America, and interestingly, they did not show much seasonal difference.

4. Summary and Discussions

[22] A global map of measurement uncertainties in satellite-based precipitation estimates has been produced, by computing the measurement spread within an ensemble of six different TRMM-era precipitation products (3B42, 3B42RT, CMORPH, GSMaP, PERSIANN, and NRL; Table 1). Our results show that the ensemble mean reproduced the major features of global precipitation distribution consistent with existing observations, such as the ITCZ and the Indian summer Monsoon. This illustrates the promise of satellite-based global retrievals. The uncertainties among these different measurements are relatively small (40–60%) over the oceans, especially in the tropics, and over the lower-latitude South America (Figure 2).

[23] Many error features were revealed from a global perspective. For example, there are large uncertainties (100–140%) over high latitude (poleward of 40° latitude), especially during the cold season (e.g., Figure 2a for Northern and Figure 2c for Southern Hemisphere). High relative uncertainties also persisted through the seasons over complex terrains, including the Tibetan Plateau, the Rockies and the Andes (Figure 2). Coastlines and water bodies also clearly reflect large uncertainties (e.g., Figures 2b and 2c).

[24] The global relative uncertainties also exhibited fairly systematic seasonal, regional as well as rain-rate dependencies (Figure 3). In general, the stronger the precipitation, the lower are the uncertainties. Europe exhibits the largest ensemble spread in winter among the five regions studied (Figures 3c and 3f). The spread over land surfaces is close to that over ocean in summer, but higher in winter (Figure 3).

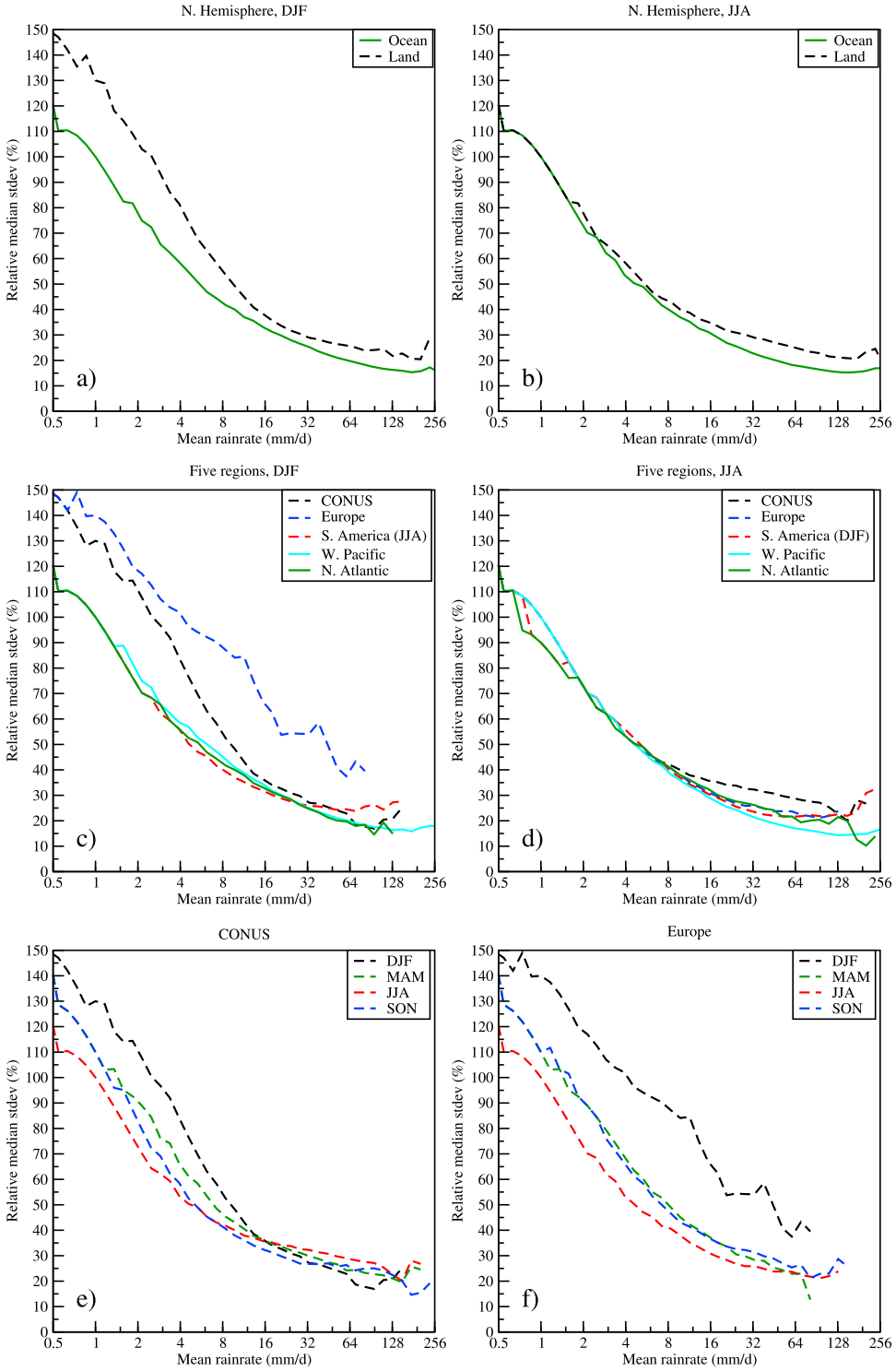

Figure 3. Standard deviation from the ensemble mean, as percentage of the mean daily precipitation at each associated rain rate bin, for Northern Hemisphere (a) winter (DJF) and (b) summer (JJA), for the five regions for (c) local winter and (d) local summer, and for the four seasons over (e) CONUS and (f) Europe.

The seasonal variation over the ocean and South America is weak.

[25] Synthesis of these results supports the belief that current satellite-based precipitation products are more reliable over areas with strong convective precipitation and flat surfaces, such as the tropical oceans and, interestingly, South America. On the other hand, complex terrains, coastlines and inland water bodies, cold surfaces, high latitudes and light precipitation emerge as areas with larger spreads and by implication larger measurement uncertainties.

[26] We want to note that the approach used herein produces only a relative estimation of the measurement uncertainties in these data sets, because these data sets are not entirely independent measurements, thus the uncertainties

obtained via analysis of the ensemble spread should be viewed as lower-bound estimates of the total uncertainty. Nonetheless, the uncertainty map can serve as a quantitative measure of the "difficulty" of measuring global precipitation over various areas, because smaller variance among the different products reflects less sensitivity to the particular detection and rain-rate blending algorithms. We also compared our results with those of *Adler et al.* [2009] who used a three-member ensemble to derive a composite climatology in the tropics, and their results showed much lower uncertainties because of their much lower temporal and spatial resolutions (monthly and 0.5°). Moreover, we examined Figure 3 against the analytically derived results of *Huffman* [1997] and found the curves in Figure 3, when plotted in the same linear scale (not shown), are very similar to those of *Huffman* [1997], except that his values are systematically lower also due to the much coarser resolution (2.5°).

[27] In addition, the ensemble membership is not large, and each one of them is not bias-free relative to the ensemble mean. Therefore, some systematic errors may be realized as the random errors in our approach. However, this will not affect our conclusion because they only increase the ensemble spread.

[28] **Acknowledgments.** This research is partially supported by the Air Force Weather Agency (AFWA) MIPR F3HRA19027G001 (PI: C. Peters-Lidard). The authors wish to thank John Eylander at AFWA for program support, and George Huffman, Robert Adler, Robert Joyce, John Janowiak, Takuji Kubota, Tomoo Ushio, F. Joseph Turk, and Kuo-lin Hsu for their efforts in producing and providing the respective data sets. Helpful comments from George Huffman and an anonymous reviewer are greatly appreciated.

References

Adler, R. F., A. J. Negri, P. R. Keehn, and I. M. Hakkarinen (1993), Estimation of monthly rainfall over Japan and surrounding waters from a combination of low-orbit microwave and geosynchronous IR data, *J. Appl. Meteorol.*, *32*, 335–356, doi:10.1175/1520-0450(1993)032<0335:EOMROJ>2.0.CO;2.

Adler, R. F., C. Kidd, G. Petty, M. Morissey, and H. M. Goodman (2001), Intercomparison of global precipitation products: The Third Precipitation Intercomparison Project (PIP-3), *Bull. Am. Meteorol. Soc.*, *82*, 1377–1396, doi:10.1175/1520-0477(2001)082<1377:IOGPPT>2.3.CO;2.

Adler, R. F., J.-J. Wang, G. Gu, and G. J. Huffman (2009), A ten-year tropical rainfall climatology based on a composite of TRMM products, *J. Meteorol. Soc. Jpn.*, *87A*, 281–293, doi:10.2151/jmsj.87A.281.

Ebert, E. E., J. E. Janowiak, and C. Kidd (2007), Comparison of near real time precipitation estimates from satellite observations and numerical models, *Bull. Am. Meteorol. Soc.*, *88*, 47–64, doi:10.1175/BAMS-88-1-47.

Gottschalck, J., J. Meng, M. Rodell, and P. Houser (2005), Analysis of multiple precipitation products and preliminary assessment of their impact on Global Land Data Assimilation System land surface states, *J. Hydrometeorol.*, *6*, 573–598, doi:10.1175/JHM437.1.

Hsu, K., X. Gao, S. Sorooshian, and H. V. Gupta (1997), Precipitation estimation from remotely sensed information using artificial neural networks, *J. Appl. Meteorol.*, *36*, 1176–1190, doi:10.1175/1520-0450(1997)036<1176:PEFRSI>2.0.CO;2.

Huffman, G. J. (1997), Estimates of root-mean-square random error for finite samples of estimated precipitation, *J. Appl. Meteorol.*, *36*, 1191–1201, doi:10.1175/1520-0450(1997)036<1191:EORMSR>2.0.CO;2.

Huffman, G. J., R. F. Adler, D. T. Bolvin, G. Gu, E. J. Nelkin, K. P. Bowman, Y. Hong, E. F. Stocker, and D. B. Wolff (2007), The TRMM multi-satellite precipitation analysis (TMPA): Quasi-global, multi-year, combined-sensor precipitation estimates at fine scales, *J. Hydrometeorol.*, *8*, 38–55, doi:10.1175/JHM560.1.

Janowiak, J. E., V. E. Kousky, and R. J. Joyce (2005), Diurnal cycle of precipitation determined from the CMORPH high spatial and temporal resolution global precipitation analyses, *J. Geophys. Res.*, *110*, D23105, doi:10.1029/2005JD006156.

Joyce, R. J., J. E. Janowiak, P. A. Arkin, and P. Xie (2004), CMORPH: A method that produces global precipitation estimates from passive microwave and infrared data at high spatial and temporal resolution, *J. Hydrometeorol.*, *5*, 487–503, doi:10.1175/1525-7541(2004)005<0487:CAMTPG>2.0.CO;2.

Kubota, T., et al. (2007), Global precipitation map using satellite-borne microwave radiometers by the GSMaP project: Production and validation, *IEEE Trans. Geosci. Remote Sens.*, *45*, 2259–2275, doi:10.1109/TGRS.2007.895337.

Lin, X., and A. Y. Hou (2008), Evaluation of coincident passive microwave rainfall estimates using TRMM PR and ground measurements as references, *J. Appl. Meteorol. Climatol.*, *47*, 3170–3187, doi:10.1175/2008JAMC1893.1.

McCollum, J. R., and R. R. Ferraro (2005), Microwave rainfall estimation over coasts, *J. Atmos. Oceanic Technol.*, *22*, 497–512, doi:10.1175/JTECH1732.1.

Okamoto, K., T. Iguchi, N. Takahashi, K. Iwanami, and T. Ushio (2005), The global satellite mapping of precipitation (GSMaP) project, *IEEE Trans. Geosci. Remote Sens.*, *8*, 3414–3416.

Sapiano, M. R. P., and P. A. Arkin (2009), An intercomparison and validation of high-resolution satellite precipitation estimates with 3-hourly gauge data, *J. Hydrometeorol.*, *10*, 149–166, doi:10.1175/2008JHM1052.1.

Tian, Y., C. Peters-Lidard, J. Eylander, R. Joyce, G. Huffman, R. Adler, K.-L. Hsu, F. J. Turk, M. Garcia, and J. Zeng (2009), Component analysis of errors in satellite-based precipitation estimates, *J. Geophys. Res.*, *114*, D24101, doi:10.1029/2009JD011949.

Turk, F. J., and S. D. Miller (2005), Toward improving estimates of remotely-sensed precipitation with MODIS/AMSR-E blended data techniques, *IEEE Trans. Geosci. Remote Sens.*, *43*, 1059–1069, doi:10.1109/TGRS.2004.841627.

Vila, D. A., L. G. G. De Goncalves, D. L. Toll, and J. R. Rozante (2009), Statistical evaluation of combined daily gauge observations and rainfall satellite estimates over continental South America, *J. Hydrometeorol.*, *10*, 533–543, doi:10.1175/2008JHM1048.1.

C. D. Peters-Lidard and Y. Tian, NASA Goddard Space Flight Center, Mail Code 614.3, Greenbelt, MD 20771, USA. (yudong.tian@nasa.gov)